Species-Specific Inhibition of Inosine 5′-Monophosphate Dehydrogenase by Mycophenolic Acid†

Jennifer A. Digits and Lizbeth Hedstrom*

Department of Biochemistry, Brandeis University, 415 South Street, Waltham, Massachusetts 02454

Received July 7, 1999; Revised Manuscript Received September 1, 1999

ABSTRACT: IMPDH catalyzes the oxidation of IMP to XMP with the concomitant reduction of NAD^+ to NADH. This reaction is the rate-limiting step in de novo guanine nucleotide biosynthesis. Mycophenolic acid (MPA) is a potent inhibitor of mammalian IMPDHs but a poor inhibitor of microbial IMPDHs. MPA inhibits IMPDH by binding in the nicotinamide half of the dinucleotide site and trapping the covalent intermediate E-XMP*. The MPA binding site of resistant IMPDH from the parasite *Tritrichomonas foetus* contains two residues that differ from human IMPDH. Lys310 and Glu431 of *T. foetus* IMPDH are replaced by Arg and Gln, respectively, in the human type 2 enzyme. We characterized three mutants of *T. foetus* IMPDH: Lys310Arg, Glu431Gln, and Lys310Arg/Glu431Gln in order to determine if these substitutions account for the species selectivity of MPA. The mutation of Lys310Arg causes a 10-fold decrease in the K_i for MPA inhibition and a 8−13-fold increase in the K_m values for IMP and NAD^+. The mutation of Glu431Gln causes a 6-fold decrease in the K_i for MPA. The double mutant displays a 20-fold increase in sensitivity to MPA. Pre-steady-state kinetics were performed to obtain rates of hydride transfer, NADH release, and hydrolysis of E-XMP* for the mutant IMPDHs. The Lys310Arg mutation results in a 3-fold increase in the accumulation level of E-XMP*, while the Glu431Gln mutation has only a minimal effect on the kinetic mechanism. These experiments show that 20 of the 450-fold difference in sensitivity between the *T. foetus* and human IMPDHs derive from the residues in the MPA binding site. Of this, 3-fold can be attributed to a change in kinetic mechanism. In addition, we measured MPA binding to enzyme adducts with 6-Cl-IMP and EICARMP. Neither of these adducts proved to be a good model for E-XMP*.

IMP dehydrogenase (IMPDH)[1] catalyzes the oxidation of IMP to XMP with the concomitant conversion of NAD^+ to NADH. This reaction is the rate-limiting step in de novo guanine nucleotide biosynthesis, and rapidly growing cells have increased levels of IMPDH (*1*). Inhibitors of IMPDH have anti-proliferative activity and are potential therapeutics for cancer. In addition, the IMPDH inhibitors ribavarin, mycophenolic acid, and mizoribine are used clinically for antiviral and immunosuppressive chemotherapy (*2*−*4*). Furthermore, there are significant differences in both kinetic parameters and inhibitor sensitivity between mammalian and microbial IMPDHs, which suggests that species-specific inhibitors could be designed for anti-infective chemotherapy (*5*−*7*).

The IMPDH reaction proceeds via attack of Cys319 (*Tritrichomonas foetus* numbering) on the 2-position of IMP, followed by hydride transfer from the E-IMP intermediate to NAD^+ (Figure 1). The resulting E-XMP* covalent intermediate is hydrolyzed to XMP, regenerating the free enzyme (*8*, *9*). The nucleophilic Cys is also targeted by IMP analogues that are inactivators, namely, 6-Cl-IMP and EICARMP (*7*, *8*, *10*, *11*). These compounds are time-dependent irreversible inhibitors of IMPDH and form covalent adducts with Cys319 as shown in Figure 2.

A number of crystal structures of IMPDH have been solved. These include structures of the Chinese hamster, human type 2, *T. foetus*, *Streptococcus pyogenes*, and *Borrelia burgdorferi* enzymes (*12*−*16*). The enzymes crystallize as a tetramer of α/β barrels. The IMPDH active site resides at the C-terminal end of the barrel β strands. The substrate and cofactor bind in a long cleft in which a stacking interaction between the IMP base and the NAD^+ nicotinamide ring facilitates hydride transfer. The highly flexible active site loop and flap also provide additional interactions at the active site cleft.

Mycophenolic acid (MPA) is a potent inhibitor of human and other mammalian IMPDHs (Figure 3). A MPA derivative, mycophenolate mofetil, is currently used as an immunosuppressive agent in the United States and Europe for organ transplantation patients (*17*, *18*). MPA is a unique inhibitor in that it is species-specific: mammalian IMPDHs are very sensitive to MPA, while IMPDHs from microbial sources are resistant to the inhibitor. For example, $K_{ii} = 10-20$ nM for human IMPDH, 9 nM for Chinese hamster

†Supported by NIH Molecular Structure and Function Training Grant GM07956 (J.A.D.), NIH GM54403 (L.H.), and a grant from the Markey Charitable Trust to Brandeis University.

* To whom correspondence should be addressed. E-mail: hedstrom@brandeis.edu. Phone: (781)736-2333. Fax: (781)736-2349.

[1] Abbreviations: IMPDH, inosine 5′-monophosphate dehydrogenase; IMP, inosine 5′-monophosphate; NAD^+, nicotinamide adenine dinucleotide; NADH, reduced nicotinamide adenine dinucleotide; XMP, xanthosine 5′-monophosphate; APAD, 3-acetylpyridine adenine dinucleotide; APADH, reduced 3-acetylpyridine adenine dinucleotide; MPA, mycophenolic acid; 6-Cl-IMP, 6-chloropurine riboside 5′-monophosphate; EICARMP, 5-ethynyl-1-β-D-ribofuranosylimidazole-4-carboxamide 5′-monophosphate; SAD, selenazole-4-carboxamide adenine dinucleotide; DTT, dithiothreitol.

10.1021/bi991558q CCC: $18.00 © 1999 American Chemical Society
Published on Web 10/29/1999

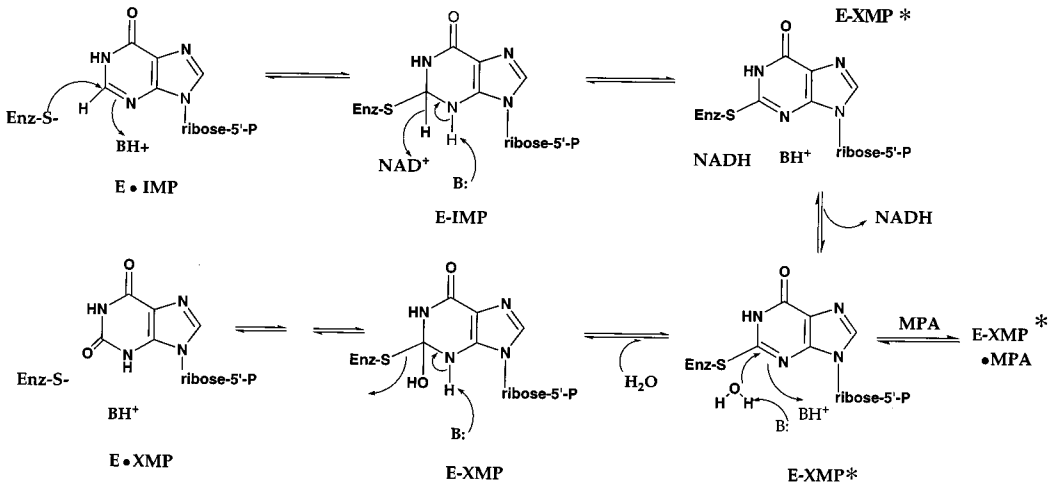

FIGURE 1: Mechanism of the IMPDH reaction.

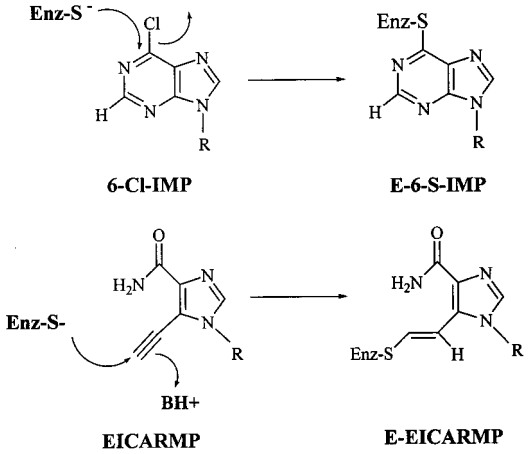

FIGURE 2: 6-Cl-IMP and EICARMP: Inactivators of IMPDH.

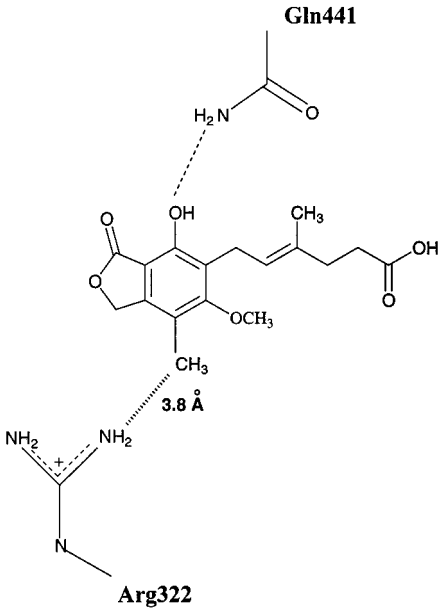

FIGURE 3: Mycophenolic acid and its interactions with Gln441 and Arg322 of Chinese hamster IMPDH.

IMPDH, 500 nM for *Bacillus subtilis* IMPDH, 7.9 μM for *B. burgdorferi* IMPDH, 14 μM for the *T. foetus* enzyme, and 20 μM for *Escherichia coli* IMPDH (*12*, *19*−*23*). MPA inhibits IMPDH by trapping the E-XMP* complex (*9*, *12*, *23*−*25*) (Figure 1). In the crystal structure of the E-XMP*•MPA complex from Chinese hamster IMPDH, MPA stacks against E-XMP* in the likely nicotinamide binding site (*12*).

The mechanism of MPA selectivity is not understood. Since MPA binds to E-XMP*, MPA sensitivity will depend on the accumulation of E-XMP* as well as the affinity of E-XMP* for MPA. Interestingly, the microbial IMPDHs have higher values of k_{cat} and K_m than their mammalian counterparts, which suggests that there is a link between MPA resistance and the kinetic properties of IMPDH (*22*, *26*−*28*).

The complete kinetic mechanism of a parasitic IMPDH, *T. foetus*, has been elucidated (Scheme 1) (*26*). It appears that only 30% of the *T. foetus* enzyme exists as E-XMP*, while E-XMP* is the predominant enzyme form in human type 2 IMPDH (*28*). Thus, only a small fraction (3-fold) of the MPA resistance of *T. foetus* IMPDH is derived from the kinetic properties of the enzyme. This observation suggests that the selectivity of MPA might be attributed to differences in the MPA binding sites. A crystal structure of Chinese hamster IMPDH (98% identical to human IMPDH) in which MPA is bound to E-XMP* reveals several residues making contact with MPA (*12*). Of these, Arg322 and Gln441 are not conserved among the microbial IMPDHs (Figure 3). The corresponding residues in *T. foetus* IMPDH are Lys310 and Glu431.

We have constructed and characterized six mutants of IMPDH with the goal of identifying structural features that determine species selectivity of MPA. In the human type 2 IMPDH, we constructed Arg322Lys, Gln441Glu, and Arg322Lys/Gln441Glu with the hope of gaining resistance to MPA. Unfortunately, these mutants were too inactive to charaterize thoroughly. In the *T. foetus* IMPDH, we constructed Lys310Arg, Glu431Gln, and Lys310Arg/Glu431Gln with the expectation of gaining sensitivity to MPA. These enzymes are 10−20-fold more sensitive to MPA, which suggests that these residues are structural determinants of MPA sensitivity.

MATERIALS AND METHODS

Materials. IMP, APAD, MPA, and Tris were purchased from Sigma. NAD^+ was purchased from Boehringer Mannheim. 6-Cl-IMP was from Apex Organics (U.K.). DTT was purchased from Research Organics, Inc. Glycerin, EDTA, and KCl were purchased from Fisher. EICARMP was the

Scheme 1: Kinetic Scheme for *T. foetus* IMPDH

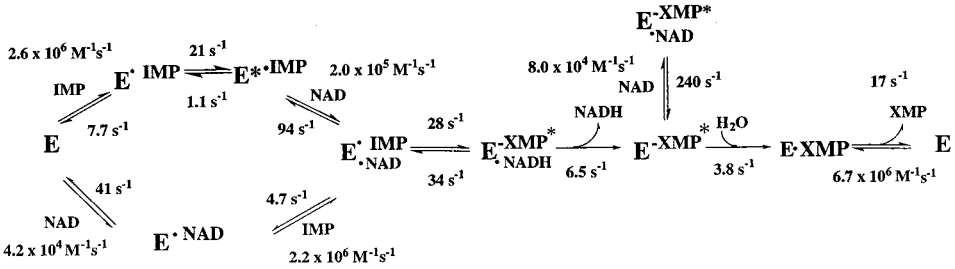

gift of Dr. Akira Matsuda. ^{3}H-labeled MPA was obtained from Moravek Biochemicals, Inc. Oligonucleotides were obtained from the Brandeis Oligonucleotide Facility.

Mutagenesis. Lys310Arg, Glu431Gln, and Lys310Arg/Glu431Gln were constructed from pTf1 using the Quikchange kit (Stratagene, La Jolla, CA) (*26*). Similarly, Arg322Lys, Gln441Glu, and Arg322Lys/Gln441Glu were constructed from pHIA5 (*19*). To ensure no undesired mutations had been introduced, the coding sequences of all IMPDH genes were sequenced using a PRISM Dyedeoxy Terminator Cycle sequencing kit (Applied Biosystems, Inc.) and an Applied Biosystems 373A DNA sequencer at the Brandeis Sequencing Facility.

Expression and Purification of IMPDH. Plasmids containing the mutant IMPDH genes were purified from an *E. coli* expression system using Cibacron blue affinity resin and cation exhange chromatography as previously described (*26*). The enzyme preparations were >95% pure as judged by SDS−PAGE. Protein concentration was measured using the Bio-Rad assay with IgG as a standard. Active sites were titrated with EICARMP (*7*).

Enzyme Kinetics. Standard IMPDH assays contained 100 mM KCl, 3 mM EDTA, 1 mM DTT, and 50 mM Tris, pH 8.0 (assay buffer). The production of NADH was monitored spectrophotometrically at 340 nm ($\epsilon = 6.22$ mM^{-1} cm^{-1}) at 25 °C using a Hitachi U-2000 spectrophotometer. The production of APADH was monitored at 363 nm ($\epsilon = 9.1$ mM^{-1} cm^{-1}). The concentrations of IMP and NAD$^+$ or analogue were varied for K_m determinations. When substrate inhibition is observed, initial velocity data were fit to the Michaelis−Menten equation (eq 1) and uncompetitive substrate inhibition equation (eq 2) using Kaleidagraph software (Abelbeck Software):

$$v = V_m[\text{IMP}]/(K_a + [\text{IMP}]) \quad (1)$$

$$v = V_m[\text{dinucleotide}]/(K_b + [\text{dinucleotide}] + [\text{dinucleotide}]^2/K_{ii}) \quad (2)$$

where v is the initial velocity; V_m is the maximal velocity; K_a and K_b are the Michaelis constants of IMP and dinucleotide, respectively; and K_{ii} is the substrate inhibition constant for dinucleotide. Steady-state parameters with respect to NAD$^+$ were derived by first determining the apparent values of V_m for the initial velocity versus IMP plots (eq 1) and replotting these values against NAD$^+$ concentration (eq 2). Similarly, the K_m value of IMP was derived by first determining the apparent values of V_m for the initial velocity versus NAD$^+$ plots using eq 2 and replotting these values against IMP concentration (eq 1). Steady-state parameters with respect to APAD were derived from initial velocity versus APAD plots at saturating IMP concentrations. In the absence of substrate inhibition, data were fit to a sequential mechanism (eq 3) using KinetAsyst software (Intellikinetics):

$$v = V_m[\text{A}][\text{B}]/(K_{ia}K_b + K_a[\text{B}] + K_b[\text{A}] + [\text{A}][\text{B}]) \quad (3)$$

where v is the initial velocity; V_m is the maximal velocity; [A] is IMP; [B] is NAD$^+$ or analogue; K_a and K_b are the Michaelis constants of IMP and NAD$^+$ or APAD, respectively; and K_{ia} is the dissociation constant of E·IMP.

Pre-steady-state experiments were performed on an Applied Photophysics SX.17MV stopped-flow spectrophotometer at 25 °C. The production of NADH was monitored either by fluorescence (excitation wavelength 340 nm, 420 nm cutoff emission filter) or by absorbance at 340 nm. Similarly, the production of APADH was followed by fluorescence (excitation wavelength 362 nm, 450 nm cutoff emission filter) or by absorbance at 363 nm. Enzyme and substrates were diluted 2-fold in assay buffer. Concentrations indicated in the text or figure legends are the final concentrations after dilution. The time course of fluorescence or absorbance can be described by a single-exponential equation with a steady-state term (eq 4):

$$S_t = (\Delta A)e^{-k(\text{obs})t} + vt \quad (4)$$

where S_t is the signal (fluorescence or absorbance) at time t, ΔA is the amplitude of the burst, k_{obs} is the observed first-order rate constant governing the burst phase, and v is the linear rate of increase in fluorescence or absorbance during steady state.

Inhibitor Kinetics. For inhibition of both wild-type and mutant IMPDHs by MPA, the values of K_{ii} were determined with constant, saturating IMP concentrations and varied NAD$^+$ concentrations at 25 °C in assay buffer. Initial velocity data were fit using KinetAsyst software (Intellikinetics) to eq 5 for uncompetitive inhibition:

$$v = V_m B/[K_b + B(1 + I/K_{ii})] \quad (5)$$

where v is the velocity, V_m is the maximum velocity, B is the concentration of NAD$^+$, I is the concentration of MPA, K_b is the apparent Michaelis constant for B, and K_{ii} is the intercept inhibition constant.

Equilibrium Dissociation Constants (K_d). Dissociation constants for the interaction of MPA with wild-type and mutant enzymes were determined by following the quenching of intrinsic protein fluorescence. The measurements were performed on a Hitachi F-2000 fluorescence spectrophotometer at 25 °C. The excitation wavelength was 280 nm.

Inner filter effects due to the MPA were corrrected by the formula (*29*)

$$F_c = F_{obs}\ \text{antilog}[(A_{ex} + A_{em})/2] \quad (6)$$

where A_{ex} and A_{em} are the absorbances at the excitation and emission wavelengths, respectively; F_c is the corrected intensity; and F_{obs} is the measured intensity. The experiments involved successive titration of the apoenzyme solution with increasing concentrations of MPA. For binding of MPA to the IMPDH-IMP complexes, the enzymes were first incubated with saturating concentrations of IMP and then titrated with MPA. From the measured fluorescence intensity I at a given ligand concentration, fractional saturation of enzyme sites with ligand (f_a) was determined by using $f_a = (I - I_a)/(I_b - I_a)$ where I_a is the fluorescence of the apoenzyme, and I_b is the fluorescence of the enyzme when all of its binding sites are saturated with ligand. The free ligand concentration was estimated using $[\text{ligand}]_{free} = [\text{ligand}]_t - n[E]_t$, in which $[\text{ligand}]_t$ and $[E]_t$ represent the total ligand and apoenzyme concentration, respectively, and n is the number of ligand binding sites on the enzyme ($n = 1$ for monomer concentration). Kaleidagraph software was used to fit f_a and $[\text{ligand}]_{free}$ to

$$f_a = [\text{ligand}]_{free}/(K_d + [\text{ligand}]_{free}) \quad (7)$$

to give the dissociation constant, K_d.

Inactivation of Human and T. foetus IMPDHs with 6-Cl-IMP and EICARMP: Equilibrium Dissociation Constants (K_d). 6-Cl-IMP and EICARMP are irreversible inhibitors of both human and *T. foetus* IMPDHs (*7*, *8*, *10*, *11*). The inactivators were added in excess to the enzymes and allowed to react until the enzymes had no remaining activity. The reactions were dialyzed extensively against 50 mM Tris, pH 7.5, and 1 mM DTT to remove free inactivator. The dissociation constants for MPA binding to the *T. foetus* E-6-S-IMP and E-EICARMP complexes were determined by following the quenching of intrinsic protein fluoresecence as described above (eq 7). Since the human enzyme has no tryptophans, equilibrium dialysis was used to determine the dissociation constants for the interaction of MPA with the human complexes. For E-6-S-IMP, binding experiments were performed by ultrafiltration (*30*, *31*) using Microcon-30 filtration devices (Amicon). ^{3}H-labeled MPA was mixed with the E-6-S-IMP complex and incubated for 20 min at 25 °C in assay buffer to reach equilibrium. The tubes were spun for 1 min at 3000*g* to separate part of the unbound MPA from the mixture. An aliquot of the retentate and filtrate was taken and counted using a scintillation counter. The total enzyme concentration $[\text{E-6-S-IMP}]_t$ and total MPA concentration $[\text{MPA}]_t$ were known, and the bound MPA was measured by the difference in counts between the retente and filtrate. $[\text{E-6-S-IMP}]_f$ and $[\text{MPA}]_f$ were calculated from the difference between the total and bound concentrations. $[\text{MPA}]_f$ could also be measured from the filtrate counts. Both methods gave consistent results. The K_d was calculated according to

$$K_d = [\text{E-I}]_f[\text{MPA}]_f/[\text{E-I}\cdot\text{MPA}] \quad (8)$$

where $[\text{E-I}]_f$ is the free E-6-S-IMP concentration and [E-I·MPA] is the bound concentration. The final number is an average of several independent reactions. For E-EICARMP, binding experiments were performed using a Micro Equilibrium Dialyser device (Sialomed, Inc.) with a 25-kDa cutoff membrane. ^{3}H-labeled MPA was placed on one side of the chamber that was separated by the membrane from the E-EICARMP, which was placed on the other side of the chamber. The whole unit was constantly shaken at 25 °C and allowed to reach equilibrium. Once equilibrium was reached, an aliquot was taken from each chamber, and the amount of bound MPA was determined by radioactive counts and calculated as above (eq 8).

RESULTS

Construction of Mutant IMPDHs. The mutant enzymes were constructed and purified as described under Materials and Methods. All mutant enzymes have purification characteristics similar to wild-type IMPDH. The three human type 2 IMPDH mutants, Arg322Lys, Gln441Glu, and Arg322Lys/Gln441Glu, could not be further characterized because of their low activity (<0.045% of wild-type IMPDH activity). The *T. foetus* IMPDH mutants were active and characterized, as described below.

Characterization of Mutant IMPDHs: MPA Inhibition. The K_{ii} values for MPA inhibition of wild-type and mutant *T. foetus* IMPDHs are summarized in Table 1. In all cases, the data best fit to an uncompetitive inhibition mechanism versus NAD^+. However, the fit to a noncompetitive mechanism is only slightly worse than the uncompetitive fit. The inhibition constant for wild-type IMPDH is similar to that reported elsewhere (*23*). MPA is also an uncompetitive inhibitor of the human enzyme. This value was determined previously using an equation that describes a tight binding uncompetitive inhibitor and is similar to other reported values (*19*, *20*). The K_{ii} for MPA inhibition is decreased 10-fold for Lys310Arg IMPDH and 6-fold for the Glu431Gln enzyme as compared to the wild-type IMPDH. The double mutant exhibits a 20-fold increase in its sensitivity to MPA as compared to wild-type IMPDH. However, this mutant enzyme is still 25-fold more resistant to MPA than human IMPDH (Table 1).

Steady-State Kinetics. The steady-state parameters for the mutant enzymes are shown in Table 1. In Lys310Arg, k_{cat} is increased 2.5-fold relative to wild-type, the K_m for IMP is increased 8-fold, and the K_m for NAD^+ is increased 13-fold. Interestingly, the value of K_m for APAD is 27-fold lower than that of NAD^+.

Although the Glu431Gln enzyme has a lower value of K_{ii} for MPA, it exhibits only modest (≤3-fold) changes in the steady-state kinetic parameters as compared to wild-type IMPDH. The analogous mutation in *S. pyogenes* IMPDH also exhibits wild-type activity, although the substitution of Gln441 with Ala in the Chinese hamster IMPDH decreases the k_{cat}/K_m by 96% (*12*, *15*).

As in the case of the Glu431Gln IMPDH, the double mutant enzyme also displays small changes (≤3.8-fold) in the steady-state parameters as compared to wild-type IMPDH. Here, the value of K_m for APAD is 7-fold lower than that of NAD^+. Thus, like the Lys310Arg enzyme, the double mutant IMPDH also prefers APAD over NAD^+.

Pre-Steady-State Kinetics Measured by Absorbance. The pre-steady-state kinetics of wild-type *T. foetus* IMPDH have

Table 1: Michaelis−Menten Parameters for Wild-Type and Mutant *T. foetus* IMPDH[a]

enzyme	dinucleotide substrate	K_m IMP (μM)	K_m dinucleotide (μM)	K_{ii} dinucleotide (mM)	k_{cat} (s^{-1})	IMP V/K_m (M^{-1} s^{-1}) $\times 10^5$	dinucleotide V/K_m (M^{-1} s^{-1}) $\times 10^4$	K_{ii} MPA (μM)
wild-type	NAD^+	1.7 ± 0.4[b]	150 ± 30[b]	6.8 ± 1.8[b]	1.9 ± 0.2[b]	11 ± 3[b]	1.3 ± 0.3[b]	9.0 ± 0.5
	APAD	5.3 ± 0.4[b]	450 ± 160[b]	na[b]	3.8 ± 0.3[b]	7.2 ± 1.4[b]	0.85 ± 0.27[b]	7.6 ± 0.5
K310R	NAD^+	14 ± 2	1900 ± 300	na[e]	4.9 ± 0.3	3.5 ± 0.4	0.26 ± 0.03	0.88 ± 0.05
	APAD		70 ± 10	18 ± 4	2.4 ± 0.1		3.4 ± 0.3	
E431Q	NAD^+	2.2 ± 0.8	106 ± 6	8.3 ± 0.8	0.6 ± 0.01	2.7 ± 1.1	0.57 ± 0.04	1.6 ± 0.1
	APAD		400 ± 36	16 ± 2	1.3 ± 0.05		0.33 ± 0.056	0.95 ± 0.05
K310R/E431Q	NAD^+	5 ± 2	500 ± 180	na[e]	0.52 ± 0.04	1.1 ± 0.39	0.1 ± 0.03	0.5 ± 0.04
	APAD		67 ± 10	18.8 ± 4	0.62 ± 0.02		0.93 ± 0.15	0.67 ± 0.03
human	NAD^+	4 ± 1[c]	6 ± 1[c]	590 ± 20[c]	0.39 ± 0.01[c]	0.98 ± 0.14[c]	6.5 ± 0.5[c]	0.022 ± 0.008[d]
	APAD	34 ± 5[c]	30 ± 5[c]	na[c]	0.62 ± 0.05[c]	0.23 ± 0.02[c]	2.1 ± 0.2[c]	

[a] Reactions were performed in 100 mM KCl, 50 mM Tris, pH 8.0, 1 mM DTT, and 3 mM EDTA at 25 °C. Absorbance was monitored as described in Materials and Methods. na, not applicable. [b] These values are from ref *26*. [c] These values are from ref *28*. [d] This value is from ref *19*. [e] No substrate inhibition is observed at $[NAD^+] \leq 8$ mM.

Table 2: Pre-Steady-State Kinetics Monitored by Absorbance and Fluorescence[a]

enzyme	dinucleotide	k_{burst}[b] (s^{-1})	k_{fluor}[c] (s^{-1})	[NADH]/$[E]_t$[d]
wild-type[e]	NAD^+	62 ± 6	6.5 ± 0.3	0.45 ± 0.1
	APAD	≥ 415	≥ 60	0.80 ± 0.10
K310R	NAD^+	≥ 170[f]	≥ 64[g]	1.0 ± 0.1
	APAD		≥ 3.3[h]	
E431Q	NAD^+	25 ± 6.5	0.96 ± 0.10	0.4 ± 0.02
	APAD		≥ 4.9[h]	
K310R/E431Q	NAD^+	5.5 ± 1.5	4.4 ± 0.4	1.1 ± 0.1
	APAD		5.5 ± 1.5	

[a] The time course of absorbance and fluorescence can be described by a single-exponential equation with a steady-state term. The rate constant for the exponential phase is k_{obs}. [b] These values are for E·IMP as the beginning complex. The rate constants for k_{obs} display a hyperbolic dependence on $[NAD^+]$. Using eq 9 in the text, the maximum value, k_{burst}, can be determined. [c] These values are for E·IMP as the beginning complex. The rate constants for k_{obs} display a hyperbolic dependence on $[NAD^+]$ and [APAD]. Using eq 9 in the text, the maximum value, k_{fluor}, can be determined. [d] [NADH] is obtained from $\Delta A_{340}/\epsilon l$, where ΔA_{340} is the amplitude of the burst, ϵ is 6.22 mM^{-1} cm^{-1} for NADH, and l is the path length (1 cm). [e] These values are from ref *26*. [f] The rate constant for the exponential phase is linearly dependent on NAD^+ up to concentrations of 20 mM, $k_{obs} = 42$ s^{-1}. This concentration of NAD^+ is approximately one-fourth of the K_{app} (eq 9). [g] The rate constant for the exponential phase is linearly dependent on NAD^+ up to concentrations of 15 mM, $k_{obs} = 12.8$ s^{-1}. This concentration of NAD^+ is approximately one-fifth of the K_{app} (eq 9). [h] Values of k_{obs} at [APAD] = 20 mM. Therefore, these values are lower limits on k_{fluor}.

been thoroughly characterized (*26*). A burst of NADH production is observed when absorbance is monitored. An isotope effect is observed on this burst phase when 2-^{2}H IMP is the substrate, which implies that hydride transfer is rate-limiting in this phase. This observation suggests that the rate constant for the burst phase (k_{burst}, Table 2) represents the hydride transfer step. Furthermore, only ~0.5 equiv of NADH is produced per active site. This burst amplitude is <1 because the hydride transfer step is at equilibrium due to the slower NADH release step (*26*).

As with the wild-type IMPDH, a pre-steady-state burst of NADH is observed for the mutant IMPDHs. Figure 4A shows a representative experiment with Glu431Gln. Here, as with the other mutants, the enzyme was preincubated with saturating IMP and mixed with NAD^+, and the data were fit to a single-exponential equation with a steady-state term (eq 4). As shown in Figure 4B, the rate constants for the

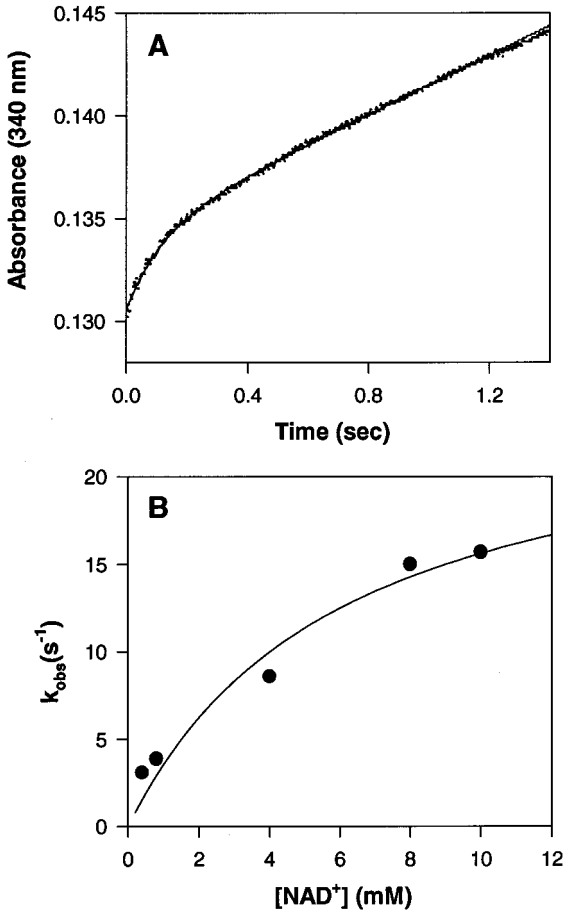

FIGURE 4: Pre-steady-state burst of NADH production as determined with absorbance. (A) This trace shows the approach to the steady-state rate obtained when 2.0 μM Glu431Gln enzyme was preincubated with 100 μM IMP and mixed with 4 mM NAD^+ under assay conditions (see Materials and Methods). The line is a fit of the data to eq 4 in the text. (B) Dependence of k_{obs} on NAD^+ concentration. The data were fit to eq 9 to obtain the value of k_{burst}.

exponential phase, k_{obs}, display a hyperbolic dependence on NAD^+ concentration. The maximum value of k_{obs}, denoted k_{burst}, was calculated according to eq 9 for Glu431Gln and the other mutants and is shown in Table 2:

$$k_{obs} = k_{burst}[NAD^+]/(K_{app} + [NAD^+]) \qquad (9)$$

where K_{app} is the concentration of varied substrate at one-half of the maximum value of k_{burst}.

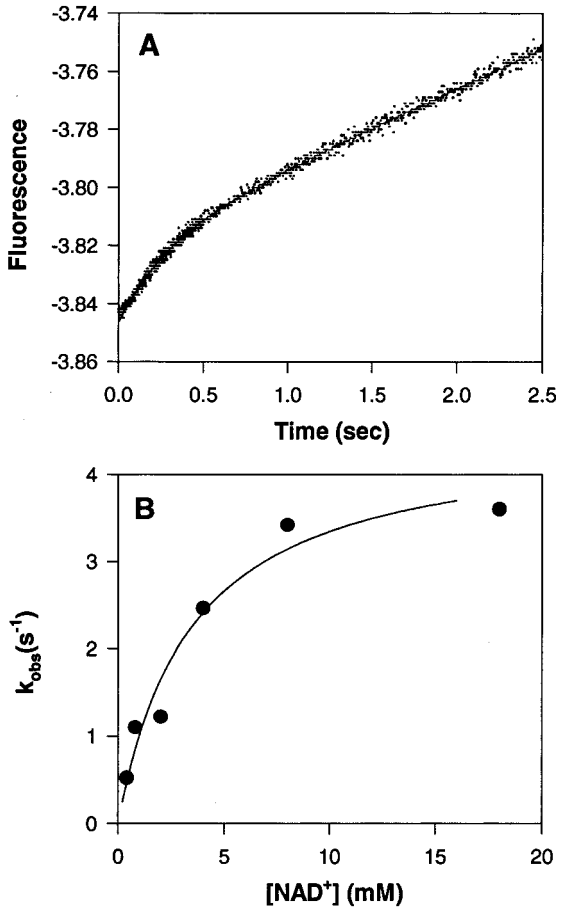

FIGURE 5: Pre-steady-state burst of NADH production as determined with fluorescence. (A) This trace shows the approach to the steady-state rate obtained when 0.5 μM Lys310Arg/Glu431Gln enzyme was preincubated with 200 μM IMP and mixed with 18 mM NAD^+ under assay conditions. The line is a fit of the data to eq 4 in the text. (B) Dependence of k_{obs} on NAD^+ concentration. The data were fit to eq 9 to obtain the value of k_{fluor}.

In Lys310Arg, the rate of hydride transfer is at least 2.7-fold greater than that of the wild-type enzyme, while in Glu431Gln, it is 2.5-fold lower relative to the wild-type IMPDH. Interestingly, the double mutant has a much lower hydride transfer rate than both single mutants and is 12-fold lower than that of the wild-type enzyme.

Pre-Steady-State Kinetics Measured by Fluorescence. The production of NADH can also be determined by monitoring its fluorescence signal. For wild-type IMPDH, a burst is observed when the fluorescence is monitored, but it is slower than the burst observed when absorbance is followed (*26*). We believe that the fluorescence of enzyme-bound NADH is quenched, and fluorescence is only observed when NADH is released from the enzyme. Therefore, the fluorescence burst ($k_{fluor} = 6.5\ s^{-1}$, Table 2) reflects NADH dissociation from E-XMP*·NADH.

Figure 5A shows the burst of NADH production when the Lys310Arg/Glu431Gln enzyme is preincubated with IMP and mixed with NAD^+. Here, as with the other mutants, the data were fit to a single-exponential equation with a steady-state term (eq 4). As when absorbance is monitored, the rate constants for the exponential phase, k_{obs}, display a hyperbolic dependence on NAD^+ concentration (Figure 5B). The maximum values of k_{obs}, denoted k_{fluor}, were calculated according to eq 9.

Table 3: Dissociation Constants for MPA Binding to Wild-Type and Mutant IMPDHs[a]

enzyme	beginning complex	K_d (μM)
wild-type	E	71 ± 7
	E·IMP	110 ± 7
	E-EICARMP	104 ± 2
	E-6-S-IMP	23 ± 4
K310R	E	93 ± 12
	E·IMP	74 ± 4
	E-EICARMP	
	E-6-S-IMP	
E431Q	E	59 ± 9
	E·IMP	80 ± 5
	E-EICARMP	
	E-6-S-IMP	27 ± 3
K310R/E431Q	E	73 ± 7
	E·IMP	27 ± 4
	E-EICARMP	
	E-6-S-IMP	
human	E	NB[b]
	E·IMP	6[c]
	E-EICARMP	>3.3[d]
	E-6-S-IMP	5.0 ± 1.7[e]

[a] Binding assays were performed in 100 mM KCl, 50 mM Tris, pH 8.0, 1 mM DTT, and 3 mM EDTA at 25 °C. The dissociation constants were determined by titration with MPA and monitoring the accompanying fluorescence decrease. [b] There is no appreciable binding of MPA to free Chinese hamster IMPDH (98% identical to human IMPDH) (*32*). [c] This value is from an isothermal titration calorimetry experiment performed with Chinese hamster IMPDH (*32*). [d] This value is a lower limit that was determined from the equilibrium dialysis experiment (Materials and Methods). [e] This value is from the ultrafiltration experiment (Materials and Methods).

The value of k_{fluor} in Glu431Gln IMPDH is much lower (25-fold) than the value of k_{burst}. In Lys310Arg, k_{fluor} is $\geq 64\ s^{-1}$, which is similar to the value of k_{burst}, although both numbers are lower limits. Interestingly, the value of k_{fluor} for the double mutant enzyme is identical to the value of k_{burst}.

The pre-steady-state kinetics of the APAD reaction were also determined by monitoring the production of APADH (Table 2). With the exception of Lys310Arg IMPDH, all enzymes have values of k_{fluor} which are greater than the values of k_{cat} with APAD as a substrate.

Binding of MPA to IMPDH. We examined the binding reactions between MPA and various forms of wild-type and mutant *T. foetus* IMPDHs as well as the human type 2 IMPDH (Table 3). Our goal was to find an adequate model for the E-XMP* complex. Such a model should have a value of $K_d \leq K_{ii}$ for MPA. The association of MPA with *T. foetus* IMPDH quenches its intrinsic protein fluorescence. Figure 6A shows a representative fluorescence emission spectrum of E-6-S-IMP before and after addition of MPA. The value of the dissociation constant (K_d) can be determined from the dependence of fluorescence intensity upon substrate concentration (eq 7). Figure 6B shows a binding curve in which the changes in fluorescence are represented by fractional saturation of enzyme sites with MPA as its concentration increases. Since human IMPDH does not have any tryptophan residues, the dissociation constants were determined by equilibrium dialysis and calculated by eq 8 as described under Materials and Methods.

MPA binds to wild-type *T. foetus* IMPDH (Table 3), which appears to be inconsistent with the uncompetitive mechanism of inhibition. However, the binding is relatively weak (K_d

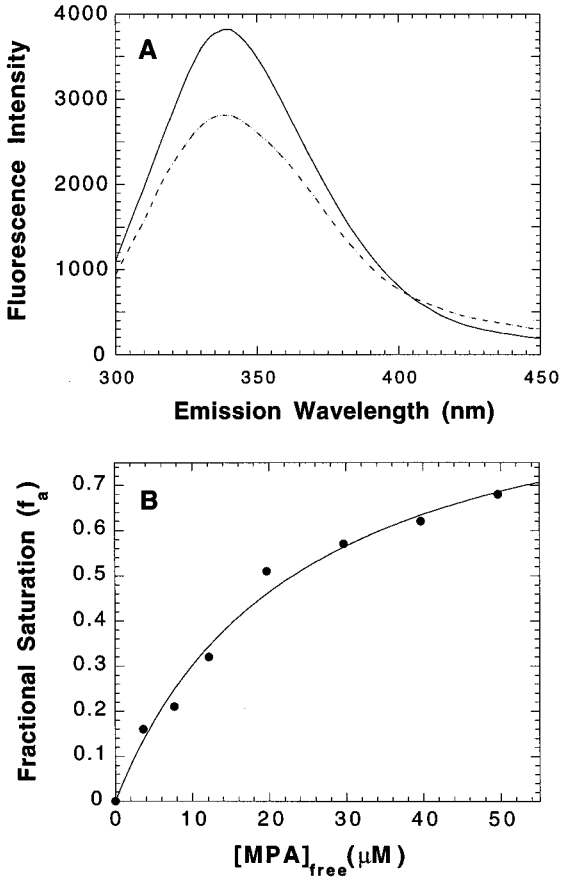

FIGURE 6: Binding of MPA to E-6-S-IMP. (A) Fluorescence emission spectra for wild-type E-6-S-IMP and its complex with MPA (dashed line) when excited with light of 280 nm; the enzyme concentration is 0.34 μM, and the MPA concentration is 20 μM. (B) Dependence of fractional saturation of the enzyme on MPA concentration as IMPDH is titrated with ligand. The data were fit to eq 7.

$= 71$ μM vs $K_{ii} = 9$ μM). The binding curve is hyperbolic (data not shown), which suggests that there is no cooperativity. Interestingly, MPA does not bind appreciably to the free Chinese hamster IMPDH (98% identical to human) (*32*). MPA binds to the mutant enzymes, with values of K_d similar to that of the wild-type IMPDH.

MPA also binds to E·IMP (Table 3). The binding curves are hyperbolic, indicating a simple, noninteracting binding reaction for each enzyme (data not shown). For the wild-type *T. foetus* enzyme, the value of K_d is 12-fold greater than the value of K_{ii} for MPA inhibition. MPA also binds noncooperatively to the Chinese hamster E·IMP complex, with a K_d of 6 μM (*32*). Since this value is 18-fold lower than that of wild-type *T. foetus* IMPDH, E·IMP does exhibit the species selectivity of E-XMP*. Interestingly, the two single mutants have similar dissociation constants as the wild-type *T. foetus* enzyme, while the double mutant has a value that falls between those of the human and the *T. foetus* IMPDHs.

The E-EICARMP covalent complex was also used for binding studies (Table 3). For wild-type *T. foetus* IMPDH, the value of K_d for the interaction of MPA with E-EICARMP is 10-fold greater than the value of K_{ii} for MPA inhibition and similar to that of E·IMP. No MPA binding was observed to the human E-EICARMP adduct.

Scheme 2: Accumulation of E-XMP*

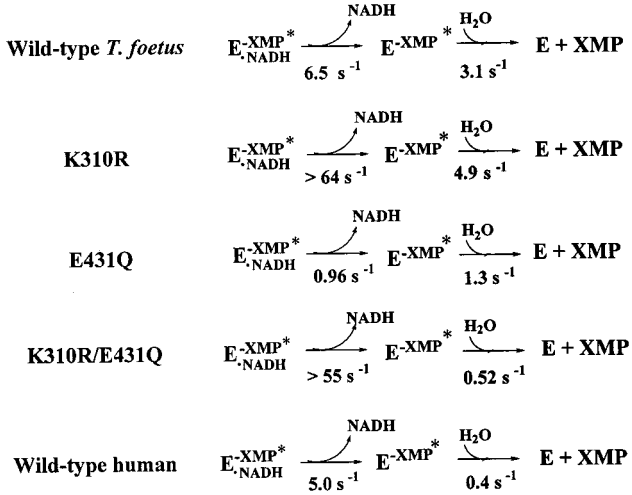

MPA also binds to the E-6-S-IMP adduct (Table 3). For wild-type *T. foetus* IMPDH, the value of K_d for the association of MPA with E-6-S-IMP is only 2.6-fold greater than the value of K_{ii} for MPA inhibition. The value of K_d for the association of MPA with the human E-6-S-IMP complex is 5-fold lower than that of the *T. foetus* enzyme. For the Glu431Gln enzyme, the value of K_d to E-6-S-IMP is similar to that of the wild-type enzyme. Interestingly, both Lys310Arg and Lys310Arg/Glu431Gln IMPDHs cannot be completely inactivated with 6-Cl-IMP, even after several days. Therefore, these dissociation constants could not be determined.

DISCUSSION

MPA is a potent inhibitor of mammalian IMPDHs but a poor inhibitor of the microbial enzymes. For example, there is a 450-fold difference in the inhibition constants between the human and *T. foetus* enzymes (20 nM and 9 μM; ref *19* and Table 1, respectively). MPA binds in the nicotinamide site and traps the E-XMP* intermediate (*9*, *12*, *23*−*25*). Therefore, the MPA affinity will depend on the accumulation of E-XMP* as well as the structure of the MPA binding site. There are significant differences in the steady-state kinetic parameters between mammalian and microbial IMPDHs. In the case of *T. foetus* IMPDH, the value of k_{cat} is 5-fold higher than for the human type 2 IMPDH, while the value of K_m for NAD^+ is 25-fold higher (*26*, *28*). Thus, differences in the accumulation of E-XMP* might account for MPA selectivity.

Analysis of the kinetic mechanisms of *T. foetus* and human type 2 IMPDH suggest that this is not the case (refs *26* and *28*; J. A. Digits and W. Wang, unpublished results). The full kinetic mechanism for *T. foetus* IMPDH is shown in Scheme 1, while an abbreviated mechanism in which the hydrolysis of E-XMP* and dissociation of E·XMP have been combined in one step is shown in Scheme 2. The main features of the mechanism are as follows: (i) Substrates bind in a random fashion. (ii) Hydride transfer is fast and reversible, with an equilibrium of 1, as determined by the burst of NADH production measured by absorbance. (iii) Product release is ordered, with NADH release preceding hydrolysis of E-XMP*. (iv) NADH release and hydrolysis of E-XMP* are both rate-limiting. The rate of NADH release is only 1.7-

fold greater than that of hydrolysis, and both of these steps can account for the value of k_{cat}. The rate constant for NADH release is determined from the burst of NADH production, as measured by fluorescence. Simulations of the mechanism using KINSIM indicate that only 30% of the *T. foetus* IMPDH exists as E-XMP*.

Preliminary experiments with human type 2 IMPDH suggest that the mechanism follows the same general outline. As in the case of *T. foetus* IMPDH, substrates bind randomly, and product release is ordered (*28*). Hydride transfer is also fast, with an equilibrium of ~ 1 (refs *28* and *33*; J. A. Digits, unpublished results). However, there is one significant difference that is shown in Scheme 2. For human IMPDH, the release of NADH is slower than hydride transfer but much faster than k_{cat} (W. Wang, unpublished results). Although the rate constant for the dissociation of E·XMP has not been measured, the presence of a solvent deuterium isotope effect of 1.9 on k_{cat} suggests that hydrolysis of E-XMP* is rate-limiting (J. A. Digits, unpublished results). Thus, the value of k_{cat} is assigned to the hydrolysis step. Since hydrolysis is completely rate-limiting, E-XMP* accumulates to a greater extent than it does in the *T. foetus* enzyme. This difference in accumulation can account for approximately 3-fold of the 450-fold difference in MPA sensitivity.

Thus, only a small fraction of the MPA resistance of *T. foetus* IMPDH is derived from the kinetic properties of the enzyme. Therefore, the structure of the MPA binding sites could account for the remaining difference in selectivity. The crystal structure of Chinese hamster IMPDH in which MPA is bound to E-XMP* reveals only two residues that are different in *T. foetus* IMPDH (*12*). The side chain atoms of Arg322 make van der Waals contacts with the methyl moiety of MPA (Figure 3). This residue is Lys310 in the *T. foetus* enzyme. The side chain of Gln441 forms a direct hydrogen bond with the MPA hydroxyl group (Figure 3). This residue is Glu431 in *T. foetus* IMPDH.

Therefore, we have constructed mutants of both human and *T. foetus* IMPDH with the goal of determining whether these residues control MPA sensitivity. Unfortunately, the mutants of the human enzyme were inactive. However, we were able to characterize the *T. foetus* mutants, Lys310Arg, Glu431Gln, and Lys310Arg/Glu431Gln.

Lys310Arg. This single mutation results in a 10-fold increase in the sensitivity to MPA (Table 1). This increase is expected since a Lys at this position would eliminate the van der Waals contact that is present in the Chinese hamster IMPDH structure (Figure 3).

The steady-state kinetic parameters are also different from those of wild type. The values of K_m for both substrates and the value of k_{cat} are significantly higher. Scheme 2 shows a partial kinetic mechanism for this mutant, which was obtained from both absorbance and fluorescence experiments as described under Results (Table 2). Here, the values of both k_{burst} and k_{fluor} are much greater than the value of k_{cat}. Thus, both hydride transfer and NADH release are fast steps for this enzyme, and the k_{cat} value of 4.9 s^{-1} (Table 1) can be assigned to the hydrolysis step. This mechanism predicts that the amplitude of the absorbance burst should be ~ 1 for the mutant enzyme, as is observed (Table 2).

Overall, it appears that this single mutation has changed the kinetic mechanism of the enzyme. The rate of NADH release is increased at least 10-fold as compared to wild-type IMPDH. Now, hydrolysis is completely rate-limiting, and 100% of the enzyme exists as E-XMP*. Therefore, 3-fold of the 10-fold increase in MPA sensitivity is derived from changes in the kinetic mechanism.

The value of k_{cat}/K_m for APAD is 70% of that of NAD^+ for wild-type IMPDH (Table 1). This result is somewhat surprising since APAD is more reactive than NAD^+ ($E^{o\prime} = -0.258$ and -0.320, respectively). Indeed, hydride transfer is much more rapid with APAD than NAD^+ (Table 2). These observations suggest that wild-type IMPDH discriminates against APAD in the binding step. In contrast, the value of k_{cat}/K_m for APAD is greater than that of NAD^+ by 13-fold in Lys310Arg IMPDH (Table 1), which suggests that residue 310 interacts with the carboxamide group of NAD^+. The structure of the E·SAD complex of human type 2 IMPDH confirms this prediction (*14*). The analogous residue, Arg322, interacts with the selenazole-4-carboxamide via a hydrogen bonding network, which includes the conserved residue Asn303. Therefore, the Lys310Arg mutation is expected to change the enzyme structure in the vicinity of the carboxamide group of NAD^+, thus changing the relative binding affinities of APAD and NAD^+. More structural information is needed to understand the change in nucleotide specificity.

Glu431Gln. This single mutation results in a 6-fold increase in MPA sensitivity. Analogously, mutagenesis studies of Chinese hamster IMPDH in which Gln441 is substituted with Ala shows a 25-fold decrease in MPA sensitivity (*12*).

The steady-state kinetic parameters for Glu431Gln are very similar to those of the wild-type enzyme (Table 1). The biggest change is the 3-fold decrease in the value of k_{cat}. A partial kinetic mechanism is shown in Scheme 2. The rate of hydride transfer (25 s^{-1}, Table 2) is much greater than the rate of NADH release from the enzyme (0.96 s^{-1}, Table 2). Therefore, hydride transfer is at equilibrium. Thus, the amplitude of the burst should be <1, as is observed (Table 2). The rate of APADH release is greater than the k_{cat} with APAD as a substrate (4.9 and 1.3 s^{-1}, respectively; Tables 1 and 2). Therefore, the value of k_{cat} for the APAD reaction can be assigned to the hydrolysis step. Overall, both the rate constants for NADH release and hydride transfer can account for the k_{cat} of 0.6 s^{-1}: $(0.96 \times 1.3)/(0.96 + 1.3) = 0.55$ s^{-1}.

As can be seen in Scheme 2, the mechanism of Glu431Gln does not look much different than that of the wild-type enzyme. In both cases, NADH release and hydrolysis are slow steps, which suggests that approximately 30% of E-XMP* accumulates for the Glu431Gln enzyme as well. Therefore, this mutant enzyme exhibits a change in inhibitor affinity without any major changes in kinetic mechanism. The 6-fold increase in MPA sensitivity must be due to structural changes at the MPA binding site.

It has been proposed that the hydroxyl group of MPA may occupy the binding site of the catalytic water that hydrolyzes E-XMP* and that Glu431 acts as a general base for activating the water (*12*, *15*). Our steady-state results suggest that this is not the case since the substitution of Glu431 with Gln decreases the rate of hydrolysis of E-XMP* by only 3-fold.

Lys310Arg/Glu431Gln. As can be seen in Table 1, this mutant displays a 20-fold increase in its sensitivity to MPA, which is only 2-fold greater than either single mutation. Thus, these mutations are not additive.

As for the Glu431Gln enzyme, the steady-state parameters are not significantly different from those of the wild-type enzyme. Interestingly, the pre-steady-state data does differ. Scheme 2 shows a partial kinetic mechanism of the double mutant. Here, the value of k_{burst} (5.5 s^{-1}, Table 2) is identical to the value of k_{fluor} (4.4 s^{-1}, Table 2). Since these two rates are the same, both must represent the hydride transfer step. This implies that the rate of NADH release must be faster than hydride transfer by at least 10-fold. Therefore, hydride transfer is not at equilibrium. This mechanism predicts that the amplitude of the burst should be 1. This prediction is observed (Table 2). The rate of APADH release is greater than the k_{cat} with APAD as a substrate (5.5 and 0.62 s^{-1}, respectively; Tables 1 and 2). In addition, the k_{cat} for the APAD reaction is identical to the value of k_{cat} for the NAD^+ reaction. Thus, the k_{cat} value can be assigned to the hydrolysis step.

Scheme 2 shows that, for the double mutant, hydrolysis is completely rate-limiting, which suggests that all of the enzyme accumulates as E-XMP*. Therefore, 3-fold of the 20-fold increase in MPA sensitivity can be attributed to a change in kinetic mechanism. Interestingly, this mutant has a 10-fold faster rate constant for the dissociation of NADH than the human enzyme and a very similar hydrolysis rate, yet is not as sensitive to MPA as the human enzyme. This observation implies that there are other structural features that differ between these two species of IMPDH, which account for the remaining discrepancies in sensitivity. Some of these possibilities are discussed below.

Potential Models for E-XMP: MPA Binding.* We wanted to find a model for the E-XMP* complex to obtain a direct determination of the K_d for MPA. A good model for E-XMP* would have a value of $K_d \leq K_{ii}$ for MPA. Unfortunately, we were unable to identify a good model.

The E·IMP complex lacks the covalent bond between the active site Cys319 and the 2-position of IMP but can conceivably form the stacking interactions between MPA and the purine base that are observed in the Chinese hamster E-XMP*·MPA structure (*12*). However, the values of K_d are too large for E·IMP to be considered a good model. EICARMP forms a covalent adduct with the enzyme but lacks the stacking interaction (Figure 2). We could not detect any appreciable binding of MPA to the human E-EICARMP adduct. The simplest explanation for the lack of affinity of MPA for this complex is that an intact purine ring system that facilitates stacking interactions with MPA is required for adequate binding. E-6-S-IMP is a covalent adduct with an intact purine ring system (Figure 2). The 6-S-IMP binds in the same site occupied by the IMP in the E-XMP*·MPA complex of the Chinese hamster enzyme, and the conformation of 6-S-IMP is similar to that of E-XMP* (*14*). However, formation of the C6−Cys adduct requires nucleophilic attack by the Cys on the opposite side of the purine ring from the C2 position. Although 12 of the 16 residues contacting MPA are still present in this adduct, E-6-S-IMP failed to bind MPA with high affinity. Although none of these complexes proved to be a good model for E-XMP*, they confirm the increase in MPA sensitivity of the mutant enzymes.

Possible Distal Structural Determinants of MPA Sensitivity. We have demonstrated that the two residues directly in the MPA binding site can account for approximately 20-fold of the 450-fold difference in selectivity between the *T. foetus* and human enzymes. This suggests that other regions of the protein must contribute to the MPA selectivity. Since IMP contacts MPA, the IMP binding site is a candidate. However, this region is conserved among all IMPDHs. Therefore, it is not a structural determinant of MPA selectivity. Two neighboring regions are also likely candidates. The active site loop (residues 314−324 in *T. foetus* IMPDH) could confer MPA selectivity. This loop appears to be very flexible, and this mobility may be required for the transformations between E-IMP, E-XMP*, and E·XMP (*13*−*16*, *34*). Since MPA inhibits by binding to E-XMP*, this loop movement may be modulating its inhibition. There are three residues in or around the active site loop that are conserved among the microbial IMPDHs and differ from conserved residues among the mammalian IMPDHs: Ile313, Arg322, and Gly326 in *T. foetus* IMPDH are replaced by Met, Gln, and Ala, respectively, in the human type 2 IMPDH. A second possibility is the adenosine site. Interestingly, the adenosine end of the dinucleotide site is not conserved (*14*). Trp269, Arg241, and Ile27 of *T. foetus* IMPDH are replaced by Phe282, His253, and Thr45, respectively, in the human type 2 IMPDH. Such differences in the adenosine portion of the dinucleotide binding site may explain MPA selectivity. In addition, the terminal section of the active-site flap, comprising residues 420−437 (human IMPDH numbering), lies adjacent to the adenosine end of the dinucleotide. These residues are also not conserved among IMPDHs.

Summary. The substitution of Lys310 with Arg and Glu431 with Gln can account for 20-fold of the 450-fold difference in sensitivity between the *T. foetus* and human type 2 IMPDHs. Three-fold of this 20-fold is derived from an increase in the accumulation of E-XMP*. These results indicate that regions of IMPDH outside the MPA binding site must contribute to its selectivity.

ACKNOWLEDGMENT

We thank Rebecca Myers for the DNA sequencing.

REFERENCES

1. Weber, G. (1983) *Cancer Res. 43*, 3466−3492.
2. Streeter, D. G., Witkowski, J. T., Khare, G. P., Sidwell, R. W., Bauer, R. J., Robins, R. K., and Simon, L. N. (1973) *Proc. Natl. Acad. Sci. U.S.A. 70*, 1174−1178.
3. Robins, R. (1982) *Nucleosides Nucleotides 1*, 35−44.
4. Allison, A. C. (1993) *Immunol. Rev. 136*, 5−28.
5. Hupe, D., Azzolina, B., and Behrens, N. (1986) *J. Biol. Chem. 261*, 8363−8369.
6. Verham, R., Meek, T. D., Hedstrom, L., and Wang, C. C. (1987) *Mol. Biochem. Parasitol. 24*, 1−12.
7. Wang, W., Papov, V. V., Minakawa, N., Matsuda, A., Biemann, K., and Hedstrom, L. (1996) *Biochemistry 35*, 95−101.
8. Huete-Perez, J. A., Wu, J. C., Whitby, F. G., and Wang, C. C. (1995) *Biochemistry 34*, 13889−13894
9. Link, J. O., and Straub, K. (1996) *J. Am. Chem. Soc. 118*, 2091−2092.
10. Brox, L., and Hampton, A. (1968) *Biochemistry 7*, 2589−2596.
11. Antonino, L. C., Straub, K., and Wu, J. C. (1994) *Biochemistry 33*, 1760−1765.
12. Sintchak, M. D., Fleming, M. A., Futer, O., Raybuck, S. A., Chambers, S. P., Caron, P. R., Murcko, M. A., and Wilson, K. P. (1996) *Cell 85*, 921−930.
13. Whitby, F. G., Luecke, H., Kuhn, P., Somoza, J. R., Huete-Perez, J. A., Phillips, J. D., Hill, C. P., Fletterick, R. J., and Wang, C. C. (1997) *Biochemistry 36*, 10666−10674.

14. Colby, T. D., Vanderveen, K., Strickler, M. D., Markham, G. D., and Goldstein, B. M. (1999) *Proc. Natl. Acad. Sci. U.S.A. 96*, 3531−3536.
15. Zhang, R., Evans, G., Rotella, F. J., Westbrook, E. M., Beno, D., Huberman, E., Joachimiak, A., and Collart, F. R. (1999) *Biochemistry 38*, 4691−4700.
16. McMillan, F., Hedstrom, L., Ringe, D., and Petsko, G. Manuscript in preparation.
17. Behrend, M., Lueck, R., and Pichlmayr, R. (1997) *Transplant Proc. 29*, 2927−2929.
18. Hauser, I. A., and Sterzel, R. G. (1999) *Curr. Opin. Nephrol. Hypertens. 8*, 1−6.
19. Farazi, T., Leichman, J., Harris, T., Cahoon, M., and Hedstrom, L. (1997) *J. Biol. Chem. 272*, 961−965.
20. Carr, S., Papp, E., Wu, J., and Natsumeda, Y. (1993) *J. Biol. Chem. 268*, 27286−27290.
21. Wu, T., and Scrimgeour, K. G. (1973) *Can. J. Biochem. 51*, 1391−1398.
22. Zhou, X., Cahoon, M., Rosa, P., and Hedstrom, L. (1997) *J. Biol. Chem. 272*, 21977−21981.
23. Hedstrom, L., and Wang, C. C. (1990) *Biochemistry 29*, 849−554.
24. Wu, J. C., Carr, S. F., Antonino, L. C., Papp, E., and Pease, J. H. B. (1995) *FASEB Abstr. 9*, 472.
25. Fleming, M. A., Chambers, S. P., Connelly, P. R., Nimmersgen, E., Fox, T., Bruzzese, F. J., Hoe, F. J., Fulghem, J. R., Livingston, D. J., Stuver, C. M., Sintchak, M. D., Wilson, K. P., and Thomson, J. A. (1996) *Biochemistry 35*, 6990−6997.
26. Digits, J. A., and Hedstrom, L.(1999) *Biochemistry 38*, 2295−2306.
27. Kerr, K. M., and Hedstrom, L. (1997) *Biochemistry 36*, 13365−13373.
28. Wang, W., and Hedstrom, L. (1997) *Biochemistry 36*, 8479−8483.
29. Lakowicz, J. R. (1983) *Principles of Fluorescence Spectroscopy*, Plenum Press, New York.
30. Jaffe, E. K., Abrams, W. R., Kaempfen, H. X., and Harris, K. A. (1992) *Biochemistry 31*, 2113−2123.
31. Xiang, B., Taylor, J. C., and Markham, G. D. (1996) *J. Biol. Chem. 271*, 1435−1440.
32. Bruzzese, F., and Connelly, P. R. (1997) *Biochemistry 36*, 10428−10438.
33. Xiang, B., and Markham, G. D. (1997) *Arch. Biochem. Biophys. 348*, 378−382.
34. Hedstrom, L. (1999) *Curr. Med. Chem. 6*, 545−560.

BI991558Q